Direct Evidence of Ponderomotive Filamentation in a Laser-Produced Plasma

P. E. Young, H. A. Baldis,[a] R. P. Drake, E. M. Campbell, and K. G. Estabrook
University of California, Lawrence Livermore National Laboratory, Livermore, California 94550
(Received 24 March 1988)

We present an experiment in which the ponderomotive filamentation instability is driven in a preformed, underdense plasma. The spatial profile of the driving beam is intentionally modulated to produce a striated intensity distribution of known periodicity. Dark-field imaging is used to observe the density perturbations produced by the instability. The observed threshold intensity for perturbation wavelengths of 42 μm is approximately 3×10^{13} W/cm^2 which compares favorably with homogeneous instability theory.

PACS numbers: 52.40.Nk, 42.65.Jx, 52.35.Nx

The filamentation instability[1,2] is of particular concern in inertial-confinement-fusion applications where the symmetry of the radiation imploding the pellet is important.[3] Filamentation is of a more general interest because of its role in interacting with parametric instabilities in laser-produced plasmas; filamentation can produce local laser intensities and density gradients which are much higher than the average plasma values. Typical laser beam cross sections have large intensity variations which can seed the filamentation instability. Usually the hot spots in the beam profile are distributed randomly or in diffraction rings which can change as a function of laser power.[4] Methods are being considered which should substantially reduce the instantaneous[5] and time-averaged[6,7] intensity fluctuations, but one would like to know how large a fluctuation level one can tolerate. To date, there has been a lack of quantitative comparison between experiments and predicted thresholds.

In the experiment discussed in this Letter, filamentation is driven in a preformed, underdense plasma by irradiating it with a second beam which has a well-defined spatial intensity perturbation that dominates the intrinsic intensity noise of the beam profile. We are able to identify growth of the imposed perturbation by looking for density structures with an identical wavelength. For a particular set of plasma parameters we have found an experimental threshold for ponderomotive filamentation which compares favorably with a homogeneous instability theory.

In previous work, indirect identification of filaments, such as x-ray photographs,[8-11] imaging of backscattered light,[12] angular distribution of $\frac{3}{2}\omega$ emission,[13] and imaging and angular distribution of 2ω emission,[14,15] are unsatisfactory since the relation between these processes and filaments is unclear. Direct identification of filaments with use of interferometry and shadowgraphy,[16-18] has not distinguished between filamentation and stable perturbations of the plasma density by structure in the beam. None of the above experiments have clearly demonstrated threshold conditions. An experiment[19] in which Thomson scattering identified electron plasma waves generated at $n_c/4$ in the filament walls has suggested thresholds which are somewhat lower than predicted thermal-filamentation thresholds. None of these experiments have spatially correlated filament growth with initial intensity structure in the beam or identified an instability as either ponderomotive or thermal filamentation.

The experiment has been performed with use of the Phoenix laser facility at the Lawrence Livermore National Laboratory and is shown in Fig. 1. The plasma is formed with a 100-J, 1-ns, 1.06-μm laser pulse incident on a 1-μm-thick CH foil target. The plasma is then irradiated by the filament-driving beam which is a 100-ps, 1.06-μm laser pulse of ≤ 30 J which is timed to arrive at the target 200 ps after the peak of the plasma-forming beam, when the foil has burned through and the plasma is underdense. The spatial intensity profile of the filament-driving beam is modulated by a pair of partially reflecting plates which interfere the beam with itself to

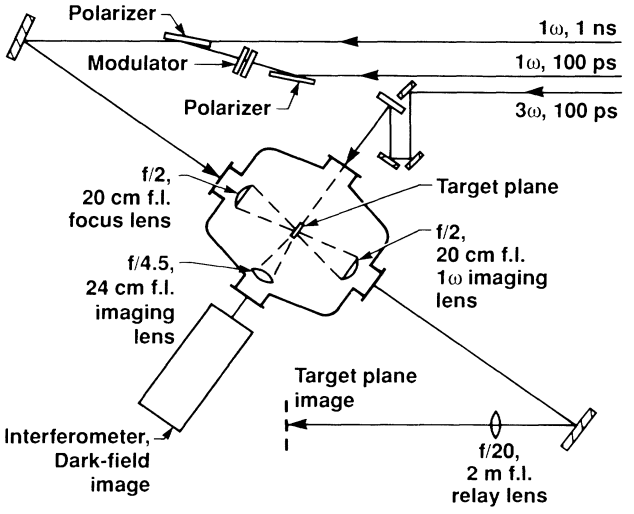

FIG. 1. Layout of the beams in the target chamber room. The 3ω probe beam can be optically delayed relative to the other two 1ω beams. A polarizer allows both the plasma-forming beam and the filament-driver beam to use the same focusing lens; the two beams have orthogonal polarizations.

produce horizontal fringes[20]; the depth of modulation can be varied by changing the reflectivity of the plates, and the perturbation wavelength can be varied by changing the angle between the plates. The peak intensity of each fringe is unchanged from the average beam intensity. In this experiment, the plate reflectivity is 40% which gives an intensity modulation of $\delta I/I_0 = 81\%$. Both the plasma-forming and filament-driving beams are focused with an $f/2$ lens and are converging at the target plane. A 100-ps, 0.35-μm probe beam is synchronized with the driving beam and aligned parallel to the fringes on the filament-driving beam and parallel to the target plane.

A principal advantage of the present experiment is that the filaments will tend to form in sheets so that a probe beam aligned tangential to the sheets will have a large path length through a filament which grows from the imposed perturbation. Because the refraction angle of a ray depends on the ratio of the path length to the density-gradient scale length,[21] we expect significant refraction of the probe beam by the sheet filaments even if they focus in width to dimensions on the order of the laser wavelength; refraction is likely to be smaller for cylindrically shaped filaments formed by hot spots since the path length through them will decrease as they focus. Dark-field imaging (DFI)[18,22] is a technique which allows one to obtain high-contrast images of the density structure by blocking the unrefracted component of the probe beam with an appropriate spatial filter located in the focal plane of the imaging lens.

The DFI imaging system consists of two lenses: The first is an $f/4.5$, 240-mm-focal-length commercial enlarger lens, while the second (not shown in Fig. 1) is an $f/1.9$, 50-mm camera lens which provides additional magnification. The total magnification is 12.7 and the resolution is 10 μm. The spatial filtering is performed in the focal plane of the second lens and consists of a pair of crossed 80-μm-diam wires oriented 45° relative to the laser axis and centered so that the intersection of the wires blocks the focus of the unrefracted probe beam. This filter rejects structures with a spatial wavelength > 150 μm in the object plane. The DFI diagnostic can relate the observed image intensity to the size of the density perturbation. The amount of refracted light is estimated by [22] $(\delta I/I_0)_p = 2(1-\cos\Delta\phi)$ with the phase shift given by $\Delta\phi \simeq (9\times10^{-22})\pi L_{p,\mu}\lambda_{p,\mu}\delta n$, where $\lambda_{p,\mu}$ is the wavelength of the probe beam (in μm), $L_{p,\mu}$ is the path length through the plasma (in μm), and δn is the size of the density perturbation in cm^{-3}.

A beam splitter after the first imaging lens relays the probe beam through a folded-beam interferometer, and then the interferrogram is imaged onto film by a relay lens identical to the one in the DFI system. The interferometer provides a measurement of the background density profile at the time that the filaments are being driven. Since the filament cross sections are so small, it is difficult to resolve fringes inside a filament and obtain a measurement of $\delta n/n$ with this diagnostic.

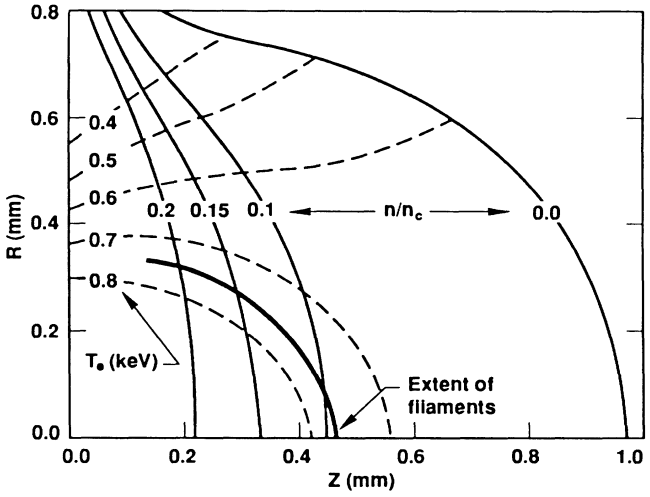

FIG. 2. Plasma density contours (solid lines) for the plasma corresponding to Fig. 3(a). The dashed lines show calculated temperature contours. The bold solid line shows the extent of the filament structure of Fig. 3(a).

The plasma parameters at the time the filament-driving beam reaches the target are shown in Fig. 2. The density profile is obtained from the interferometer while the temperature distribution is obtained from a 2D LASNEX [23] calculation. The plasma density distribution given by the code and the interferometer are in reasonable agreement at densities $\geq 0.1n_c$, but the extent of the plasma is 20% larger in the experiment. The peak density and temperature on axis are $0.25n_c$ and 1.0 keV, respectively. The absorption of the plasma is low (the inverse bremsstrahlung absorption length at $0.1n_c$ is > 9 mm), so that the filament driving beam does not significantly increase the background temperature.

An experimental estimate of the instability threshold is found from the DFI data. In Fig. 3(a), the modulated beam intensity is 4.2×10^{13} W/cm^2 (13-J, 630-μm-diam spot) and the perturbation wavelength is 42 μm; the filament structure is very evident. We expect and observe fifteen filaments. The angles of the filaments with respect to the laser axis match the angles of the incident beam. No growth is observed for driving-beam intensities as high as 2.8×10^{13} W/cm^2 (15-J, 760-μm-diam spot) and the same perturbation wavelength [see Fig. 3(b)]. In this case the plasma-forming beam is also of lower intensity because of the larger spot size, but the electron temperature will not change much with laser intensity ($T_e \propto I^{1/3}$).[24] The timing of the beams in both cases is identical. The target-plane image of the modulated beam for the case of Fig. 3(b) is shown in Fig. 3(c). Dark-field images of the preformed plasma (no modulated beam) with various spot diameters are very similar to Fig. 3(b), as are cases with the modulated beam ($I \leq 5\times10^{13}$ W/cm^2) in which the perturbation

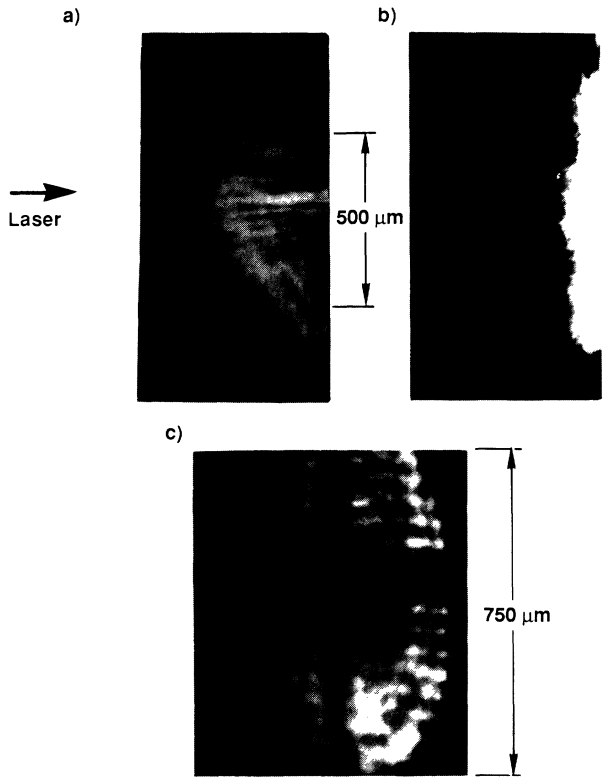

FIG. 3. Dark-field images of (a) a modulated beam of intensity $I=4.2\times10^{13}$ W/cm^2 incident on a preformed plasma, and (b) a modulated beam of intensity $I=2.8\times10^{13}$ W/cm^2 incident on a preformed plasma. (c) A television-monitor picture of the target-plane image of the modulated beam of (b).

wavelength is 135 μm. The DFI has shown only periodic structure in front of the target and only for conditions above threshold.

Figure 2 shows the location of the extent of the filament structure with respect to the plasma density and temperature distribution. Since filamentation is a nonresonant instability, we might expect reasonable predictions of threshold from a homogeneous plasma theory. Theoretical predictions[25] for the inverse growth length (Imk) of ponderomotive filamentation as a function of the perturbation wave number (Rek) are shown in Fig. 4. We can define an instability condition to exist when the laser intensity has increased one e-fold; this is indicated by the horizontal line in the graph. The ponderomotive threshold for the maximum-growth wave number k is given by[25]

$$I_p=2\times10^{15}L_\mu^{-1}\lambda_\mu^{-1}(n_c/n)T_{\rm keV}\,, \qquad (1)$$

where L_μ is the plasma length in microns, λ_μ is the laser wavelength in microns, and $T_{\rm keV}$ is the electron temperature in keV. From this formula we expect the filament to continue to grow to the peak of the density profile. LASNEX calculations show that the electron temperature

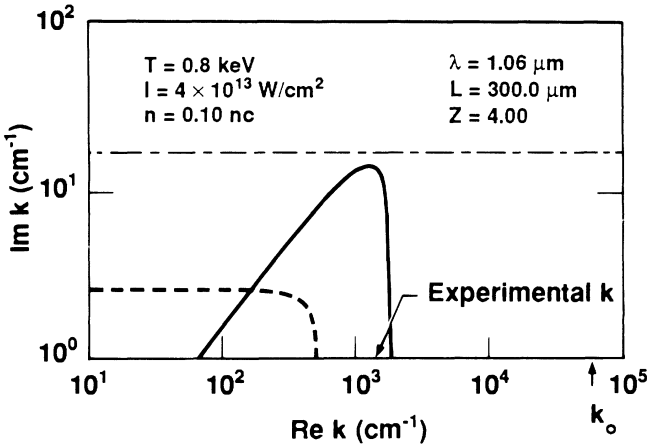

FIG. 4. Comparison of calculated thermal (dashed line) and ponderomotive (solid line) growth lengths vs instability **k** for the listed plasma parameters.

changes from 800 to 1000 eV over the same density range. For the parameters in this experiment ($L_\mu=300$ μm, $n=0.1n_c$, $T_{\rm keV}=0.8$ keV) we calculate a threshold intensity from Eq. (1) of 5×10^{13} W/cm^2. The results for a perturbation of 135 μm (no growth) are consistent with the calculated intensity threshold of 1.8×10^{14} W/cm^2. Since the parameters used in the threshold formula and the threshold criterion itself might vary by a factor of 2, one would not expect exact agreement between the calculated and experimental thresholds. It is clear, however, that there are not orders of magnitude difference between the two results. We expect that this theory accurately describes our experiment since it assumes that the light energy density is small compared to the plasma energy density. Although $\delta I/I_0$ is large, the peak intensity is low, and we will see below that the initial density perturbations are small ($\sim$0.3%).

The density perturbations are unlikely to be due to thermal filamentation. Figure 4 shows that not only is thermal filamentation predicted to be stable for the chosen plasma conditions, but it is also limited to perturbation wavelengths larger than the electron mean free path, and so for very short wavelengths only ponderomotive filamentation can grow. We can calculate the thermal threshold intensity[25] (for Rek small) to be 5×10^{15} W/cm^2, which is far above the intensity of the modulated beam.

The density perturbations to the background density n_0 due to stable intensity perturbations on the laser beam are small. The size of the density fluctuation is given by[1]

$$\delta n/n_0=(n_0-n)/n_0$$
$$=1-\exp[-0.375(v_0/v_{\rm th})^2]\,, \qquad (2)$$

where $v_0=eE_0/m\omega_0$ is the electron quiver velocity and $v_{\rm th}=(T_e/m)^{1/2}$ is the electron thermal velocity. For the parameters for the plasma of Fig. 3(a) we find (v_0/

$v_{th})^2 \simeq 0.003$ which gives a perturbation density of $\delta n/n_0 \sim 0.3\%$. Note also that v_0/v_{th} increases as one moves away from the target (because T_e decreases) which would suggest a larger $\delta n/n_0$ further away from the target; this is contrary to the observed structure. If the intensity increases to 5×10^{14} W/cm^2 because of filamentation, and assuming that T_e is unchanged, then we find $\delta n/n_0 \sim 10\%$. We estimate the peak intensity of the refracted probe-beam rays to be $(\delta I/I_0)_p \sim 50\%$. Using the expression relating to refracted probe-beam intensity to the phase shift and the phase shift to the density perturbation, we find that the observed intensity level is consistent with $\delta n/n_0 \simeq 10\%$. The increase in the density perturbation and the intensity level required to produce it are consistent with the filamentation instability.

We acknowledge support of the laser during this experiment by Jim Swain, Paul Solone, and Bill Cowens. We had useful conversations with Dr. W. L. Kruer and Dr. A. B. Langdon. Targets were provided by Ed Hsieh and the Target Fabrication Group. This work was performed under the auspices of the U.S. Department of Energy by the Lawrence Livermore National Laboratory under Contract No. W-7405-Eng-48.

---

[a]Permanent address: National Research Council of Canada, Ottawa, Ontario, Canada K1A 0R6.

[1]P. K. Kaw, G. Schmidt, and T. Wilcox, Phys. Fluids **16**, 1522 (1973).

[2]K. Estabrook, W. L. Kruer, and D. S. Bailey, Phys. Fluids **28**, 19 (1985), and references therein.

[3]J. Holtzrichter, Nature (London) **316**, 309 (1985).

[4]W. W. Simmons, D. R. Speck, and J. T. Hunt, Appl. Opt. **17**, 999 (1978).

[5]W. Seka *et al.*, Bull. Am. Phys. Soc. **32**, 1740 (1987).

[6]R. H. Lehmberg and S. P. Obenschain, Opt. Commun. **46**, 27 (1983); R. H. Lehmberg, A. J. Schmitt, and S. E. Bodner, J. Appl. Phys. **62**, 2680 (1987).

[7]Y. Kato and K. Mima, Appl. Phys. B **29**, 186 (1982), and Phys. Rev. Lett. **53**, 1057 (1984).

[8]R. A. Haas *et al.*, J. Appl. Phys. **47**, 1318 (1976).

[9]K. A. Tanaka *et al.*, Phys. Fluids **28**, 2910 (1985).

[10]T. P. Donaldson and I. J. Spalding, Phys. Rev. Lett. **36**, 467 (1976).

[11]O. Willi and P. H. Y. Lee, Opt. Commun. **55**, 120 (1985).

[12]W. C. Mead *et al.*, Phys. Fluids **27**, 1301 (1984).

[13]R. W. Short *et al.*, Phys. Rev. Lett. **52**, 1496 (1984).

[14]J. A. Stamper *et al.*, Phys. Fluids **28**, 2563 (1985).

[15]J. Meyer and Y. Zhu, Phys. Fluids **30**, 890 (1987).

[16]B. Grek *et al.*, Phys. Rev. Lett. **41**, 1811 (1978).

[17]O. Willi and P. T. Rumsby, Opt. Commun. **37**, 45 (1981).

[18]C. Joshi *et al.*, J. Appl. Phys. **53**, 215 (1982).

[19]H. A. Baldis and P. B. Corkum, Phys. Rev. Lett. **45**, 1260 (1980).

[20]F. Jenkins and H. White, *Fundamentals of Optics* (McGraw-Hill, New York, 1957), 3rd ed., pp. 270–273.

[21]F. Jahoda and G. Sawyer, in *Methods of Experimental Physics,* edited by L. Marton (Academic, New York, 1971), Vol. 9B, p. 22.

[22]M. Born and E. Wolf, *Principles of Optics* (Pergamon, New York, 1980), 6th ed., pp. 425–427.

[23]G. D. Zimmerman and W. L. Kruer, Comments Plasma Phys. Controlled Fusion **2**, 51 (1977).

[24]R. A. London and M. D. Rosen, Phys. Fluids **29**, 3813 (1986).

[25]W. L. Kruer, Comments Plasma Phys. Controlled Fusion **9**, 63 (1985).

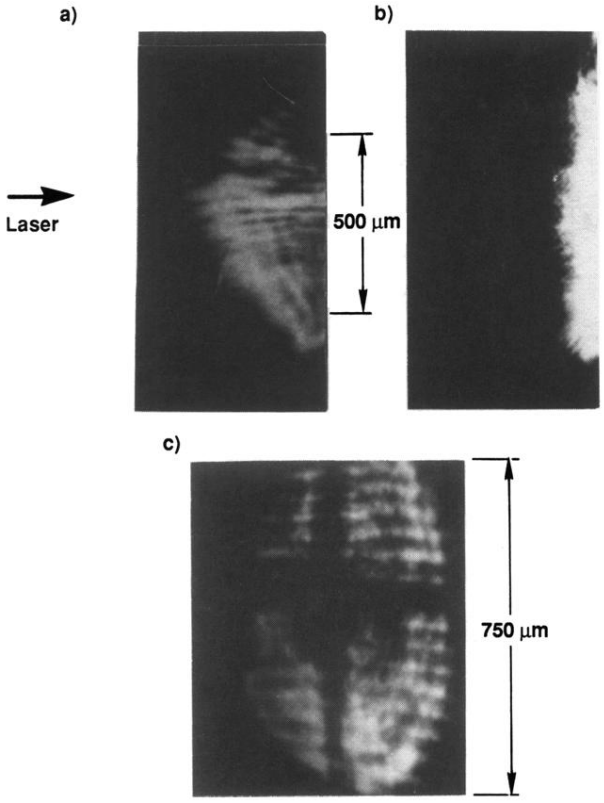

FIG. 3. Dark-field images of (a) a modulated beam of intensity $I = 4.2 \times 10^{13}$ W/cm^2 incident on a preformed plasma, and (b) a modulated beam of intensity $I = 2.8 \times 10^{13}$ W/cm^2 incident on a preformed plasma. (c) A television-monitor picture of the target-plane image of the modulated beam of (b).